Accepted Manuscript

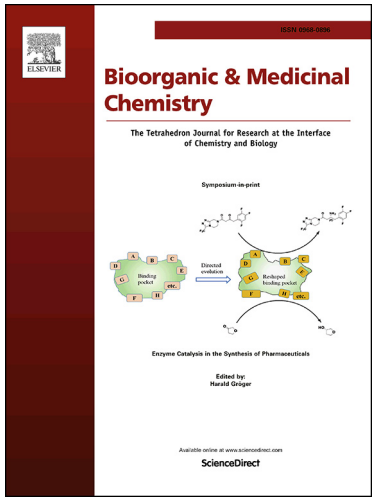

Characterization of crystal water molecules in a high-affinity inhibitor and hematopoietic prostaglandin D synthase complex by interaction energy studies

Daisuke Takaya, Koji Inaka, Akifumi Omura, Kenji Takenuki, Masashi Kawanishi, Yukako Yabuki, Yukari Nakagawa, Keiko Tsuganezawa, Naoko Ogawa, Chiduru Watanabe, Teruki Honma, Kosuke Aritake, Yoshihiro Urade, Mikako Shirouzu, Akiko Tanaka

PII: S0968-0896(18)31129-5
DOI: https://doi.org/10.1016/j.bmc.2018.08.014
Reference: BMC 14501

To appear in: *Bioorganic & Medicinal Chemistry*

Received Date: 10 July 2018
Revised Date: 7 August 2018
Accepted Date: 10 August 2018

Please cite this article as: Takaya, D., Inaka, K., Omura, A., Takenuki, K., Kawanishi, M., Yabuki, Y., Nakagawa, Y., Tsuganezawa, K., Ogawa, N., Watanabe, C., Honma, T., Aritake, K., Urade, Y., Shirouzu, M., Tanaka, A., Characterization of crystal water molecules in a high-affinity inhibitor and hematopoietic prostaglandin D synthase complex by interaction energy studies, *Bioorganic & Medicinal Chemistry* (2018), doi: https://doi.org/10.1016/j.bmc.2018.08.014

Characterization of crystal water molecules in a high-affinity inhibitor and hematopoietic prostaglandin D synthase complex by interaction energy studies

Daisuke Takaya[*,1], Koji Inaka[*,2], Akifumi Omura[*,3], Kenji Takenuki[3], Masashi Kawanishi[3], Yukako Yabuki[1], Yukari Nakagawa[1], Keiko Tsuganezawa[1], Naoko Ogawa[1], Chiduru Watanabe[1], Teruki Honma[1], Kosuke Aritake[4,5], Yoshihiro Urade[4], Mikako Shirouzu[1], and Akiko Tanaka[1**]

[1]RIKEN Center for Biosystems Dynamics Research, 1-7-22 Suehiro, Tsurumi, Yokohama 230-0045, Japan, [2]MARUWA Foods and Biosciences, Inc. 170-1 Tsutsui-cho, Yamatokoriyama, Nara 639-1123, Japan, [3]Asahi Kasei Pharma Corporation, 632-1 Mifuku, Izunokuni, Shizuoka 410-2321, Japan, [4]International Institute for Integrative Sleep Medicine (WPI-IIIS), University of Tsukuba, Tsukuba, Ibaraki 305-8575, Japan, [5]Daiichi University of Pharmacy, 22-1 Tamagawa, Minami, Fukuoka 815-8511, Japan.

[*]These authors contributed equally to this work.

[**]**Correspondence should be sent to:** Akiko Tanaka, Ph.D., RIKEN Center for Biosystems Dynamics Research, 1-7-22 Suehiro-cho, Tsurumi, Yokohama 230-0045, Japan.

E-mail: aktanaka@riken.jp, Phone: +81-45-503-9451, Fax: +81-45-503-9450

Hematopoietic prostaglandin D synthase (H-PGDS) is one of the two enzymes that catalyze prostaglandin D_2 synthesis and a potential therapeutic target of allergic and inflammatory responses. To reveal key molecular interactions between a high-affinity ligand and H-PGDS, we designed and synthesized a potent new inhibitor (K_D: 0.14 nM), determined the crystal structure in complex with human H-PGDS, and quantitatively analyzed the ligand-protein interactions by the fragment molecular orbital calculation method. In the cavity, 10 water molecules were identified, and the interaction energy calculation indicated their stable binding to the surface amino acids in the cavity. Among them, 6 water molecules locating from the deep inner cavity to the peripheral part of the cavity contributed directly to the ligand binding by forming hydrogen bonding interactions. Arg12, Gly13, Gln36, Asp96, Trp104, Lys112 and an essential co-factor glutathione also had strong interactions with the ligand. A strong repulsive interaction between Leu199 and the ligand was canceled out by forming a hydrogen bonding network with the adjacent conserved water molecule. Our quantitative studies including crystal water molecules explained that compounds with an elongated backbone structure to fit from the deep inner cavity to the peripheral part of the cavity would have strong affinity to human H-PGDS.

Key words: Hematopoietic prostaglandin D synthase; crystal water molecule; interaction energy; fragment molecular orbital method; crystal structure analysis; drug design

1 Introduction

Prostaglandin (PG) D_2, produced from arachidonic acid, is important in the pathogenesis of inflammatory diseases[1, 2] and regulation of physiological sleep.[3, 4] Hematopoietic prostaglandin D synthase (H-PGDS) is one of the two enzymes that catalyze the isomerization of PGH_2 to PGD_2. Inhibition and knockout studies of H-PGDS have indicated its involvement in allergic and inflammatory responses, and thus human H-PGDS is a potential therapeutic target.[1, 2, 5]

In 2003, Inoue et al. reported the crystal structures of human H-PGDS containing Mg^{2+} and glutathione (GSH), an essential co-factor for the enzyme.[6] The asymmetric unit of the crystal lattice contained two homodimers of H-PGDS. The monomer of H-PGDS contains a large catalytic cavity sandwiched between the N-terminal (residues 2-71) and C-terminal (residues 82-199) domains.[6] The catalytic cavity of H-PGDS is subdivided into three regions: the inner cavity surrounded by Arg14, Met99, Tyr152, and Asp96, the central cavity surrounded by Trp104, and the thioate anion of GSH, and the peripheral solvent-exposed part of the pocket.[7, 8] In 2004, the first crystal structure of human H-PGDS in complex with an inhibitor was reported.[9] Since then, many inhibitors and candidate drugs against H-PGDS have been developed and reported by pharmaceutical companies.[1, 8, 10]

In high-affinity inhibitor design, the decision of whether to engage or displace conserved water molecules is an important subject. Thus, the conserved water molecule near Leu199 in the catalytic cavity of human H-PGDS has been drawing attention.[8, 10-12] Thorarensen's group at

Pfizer reported that the complex structures of H-PGDS with nanomolar potency inhibitors all showed the hydrogen bonding between the conserved water molecule and ligands. They tried to displace the water molecule by their new ligands to enhance the binding affinity due to the entropic gain; however, they concluded that the maximal affinity for H-PGDS required ligands to form a hydrogen bonding with the water molecule.[13] Therefore, we aimed to identify all the crystal water molecules binding stably in the H-PGDS catalytic cavity and quantify their contributions to ligand binding by the fragment molecular orbital (FMO) calculation method.[14] This information will be valuable for future drug-design of high-affinity H-PGDS inhibitor molecules.

The interactions important in the ligand-protein binding are hydrophobic and electrostatic interactions, and hydrogen bonding. To understand these interactions the quantum mechanics (QM) calculation method is one of powerful approaches, because the method takes into consideration the effects of donating and withdrawing electrons and π-π interactions. The FMO method has been developed to apply the QM calculations to large biomolecules.[14-20] The method is achieved by dividing a large molecule into small pieces called fragments, such as amino acid residues, water molecules, ions, and ligands. The FMO method evaluates the electronic states of each fragment pair, and indicates their interaction magnitude in individual fragment levels with the Inter-Fragment Interaction Energy (IFIE).[21] Further, the Pair Interaction Energy

Decomposition Analysis (PIEDA) indicates the energy components of IFIE: electrostatic interaction (ES), dispersion interaction (DI), charge transfer with higher-order mixed terms energies (CT+mix), and exchange-repulsion (EX).[20, 22, 23] The ES component mainly reflects the hydrogen bonding and Coulomb interaction energies, and the DI component reflects the CH-π and π-π interaction energies. Thus ES and DI components are important for protein-ligand interactions.

In this paper, we designed and synthesized a high-affinity ligand for human H-PGDS, and then their complex crystal structure was determined. Based on the structure, FMO calculations were performed to quantify the ligand-protein interactions in fragment levels to reveal all the stably bound water molecules in the cavity and their contributions to the ligand binding.

2 Materials and methods

2.1 Synthesis of F092

2.1.1 General

First, 4-(2-oxopyrrolidin-1-yl)benzoic acid (**1**) was converted to the *N*-Boc aniline (**2**) via a Curtis rearrangement reaction under conventional conditions, and then the deprotection reaction of the Boc group was accomplished using HCl in 1,4-dioxane to produce 1-(4-aminophenyl)pyrrolidin-2-one (**3**). Subsequently, the amidation reaction of **3** and

2-(pyridin-2-yl)pyrimidine-5-carboxylic acid was performed by the addition of propylphosphonic anhydride ($T_3P^®$), to provide F092 (**4**) in good yield.

Progress of all reactions was monitored on Merck pre-coated silica gel plates using ethyl acetate (EtOAc)/hexane as a solvent system. Spots were visualized by irradiation with ultraviolet light (254 nm). Column chromatography was performed using Yamazen silica gel 60 (230 − 400 mesh). Proton (^1H) NMR spectra were recorded on a Bruker Avance 400 instrument using tetramethylsilane as an internal standard. Chemical shifts are given in parts per million (ppm) (δ relative to the residual solvent peak for ^1H). The following abbreviations are used: singlet (s), doublet (d), triplet (t), and multiplet (m). ESI mass spectrometry was performed by UPLC/MS (Waters).

2.1.2 tert-butyl (4-(2-oxopyrrolidin-1-yl)phenyl)carbamate (2).

Diphenyl phosphorazidate (DPPA) (0.251 ml, 1.2 eq.) was added dropwise to a solution of 4-(2-oxopyrrolidin-1-yl)benzoic acid (**1**) (201 mg, 1 eq.), tert-BuOH (0.93 ml, 10 eq.) and trimethylamine (Et_3N) (0.272 ml, 2.0 eq.) in toluene (4.8 ml) at room temperature (rt). The resulting pale yellow solution was stirred at 120 ºC for 16.5 h under N_2 atmosphere. The resulting brown mixture was cooled to rt and saturated $NaHCO_{3(aq)}$ (5 ml) was added to the mixture. The mixture was extracted twice with EtOAc (10 ml), and the combined organic extracts were washed with brine (5 ml), dried over $MgSO_4$, and concentrated under reduced

pressure. Purification of the crude product by flash chromatography on silica eluted with hexian-EtOAc (50:50, 30:70 and 20:80) gave **2** (183 mg, 68%) as a white solid; R_F (33:67 hexane-EtOAc) 0.45; ^{1}H NMR (400 MHz, DMSO-d_6) δ 7.51 (dd, *J* = 2.4, 2.0 Hz, 2H, Ph), 7.42 (d, *J* = 4.4 Hz, 2H, Ph), 3.78 (t, *J* = 7.2 Hz, 2H, NCH_2), 2.45 (t, *J* = 7.2 Hz, 2H, CH_2CO), 2.04 (tt, *J* = 7.2, 7.2 Hz, 2H, CH_2), 1.47 (s, 9H, *tert*-Bu); ESI-MS m/z calculated for $C_{15}H_{20}N_2O_3^+$ H^+ $[M + H]^+$; 277.2. Found: 277.3.

2.1.3 1-(4-aminophenyl)pyrrolidin-2-one (3).

To a solution of **2** (183 mg, 1.0 eq.) in 1,4-dioxane (0.67 ml) was added 4 M HCl in 1,4-dioxane (3.3 ml) at rt. The resulting solution was stirred at rt for 3 h to precipitate. Obtained precipitate was filtered, washed three times with 1,4-dioxane (5 ml), and dried under reduced pressure at 40 ºC for 18 h to give **3** (116 mg, 83%) as a white solid; ^{1}H NMR (400 MHz, DMSO-d_6) *δ* 9.99 (brs, 2H, NH_2), 7.73 (d, *J* = 8.8 Hz, 2H, Ph), 7.33 (d, *J* = 8.8 Hz, 2H, Ph), 3.83 (t, *J* = 7.2 Hz, 2H, NCH_2), 2.50 (t, *J* = 7.2 Hz, 2H, CH_2CO), 2.07 (tt, *J* = 7.2, 7.2 Hz, 2H, CH_2); ESI-MS *m/z* calculated for $C_{10}H_{12}N_2O^+$ H^+ $[M + H]^+$; 177.1. Found: 177.3.

2.1.4 N-(4-(2-oxopyrrolidin-1-yl)phenyl)-2-(pyridin-2-yl)pyrimidine-5-carboxamide (4).

A solution of propylphosphonic anhydride in EtOAc (50 wt.%, 6.45 ml, 2 eq.) was added to a solution of **3** (1.07 g, 1.1 eq.), 2-(pyridin-2-yl)pyrimidine-5-carboxylic acid (920 mg, 1.0 eq.) and Et_3N (5.10 ml, 8.0 eq.) in CH_2Cl_2 (45.7 ml) at rt. The resulting solution was stirred at rt

for 1 h to cause precipitation, which was collected by filtration and washed with EtOAc (2 x 10 ml). The obtained solid was dried under reduced pressure at 40 ºC for 18 h to give **4** (840 mg, 51%) as a white solid. Saturated $NaHCO_{3(aq)}$ was added to the filtrate, then the mixture was stirred at rt for 30 min to give a precipitate, which was collected by filtration and dried to give **4** (597 mg, 36%) as a white solid; ^{1}H NMR (400 MHz, DMSO-d_6) δ 10.67 (s, 1H, NH), 9.43 (s, 2H, NCH), 8.80 (d, *J* = 3.6 Hz, 1H, NCH), 8.47 (d, *J* = 8.0 Hz, 1H, NCH), 8.03 (t, *J* = 8.0 Hz, 1H, CH), 7.78 (d, *J* = 9.2 Hz, 2H, Ph), 7.69 (d, *J* = 9.2 Hz, 2H, Ph), 7.59 (dd, *J* = 3.6, 8.0 Hz, 1H, CH), 3.85 (t, *J* = 7.2 Hz, 2H, NCH2), 2.07 (tt, *J* = 7.2, 7.2 Hz, 2H, CH2); ESI-MS *m/z* calculated for $C_{20}H_{18}N_5O_2^+$ H^+ $[M + H]^+$: 360.1. Found: 360.3.

2.2 Purification of Histag H-PGDS

Human Histag H-PGDS was expressed and purified as described previously.[11] Briefly, the DNA fragment of the full-length H-PGDS gene (NCBI accession no.: NP 055300) fused with a 6x-Histidine tag at the N-terminus was cloned into the pET28a vector (Novagen, Madison, WI, USA) and expressed in *E. coli* one shot BL21 (DE3) (Thermo Fisher). The cells were grown in LB medium at 37 ºC, induced with 1.0 mM IPTG, and then cultured further for 4 hr at 37 ºC. The cells were collected and disrupted by sonication in 50 mM phosphate-buffer (pH 6.6), containing 2 mM $MgCl_2$, 0.4 mg/ml lysozyme, and 6 μg/ml DNase/RNase. After removal of the cell debris by centrifugation, the supernatant was filtered through a 0.45 μm PVDF filter and

applied to a GSH-Sepharose 4B column. After washing the column with 50 mM phosphate-buffer (pH 6.6) containing 2 mM $MgCl_2$, the protein was eluted with 50 mM Tris-HCl, pH 9.0 containing 10 mM GSH. The eluted H-PGDS fractions were washed three times by PBS(-) and concentrated using an Amicon Ultra filtration device. Protein concentrations were determined with a Bradford protein assay kit (Bio-Rad).

2.3 Evaluation of H-PGDS inhibitors by Surface Plasmon Resonance (SPR)

SPR spectroscopy measurement was performed at 25 ºC on a Biacore T-200 instrument (GE Healthcare Life Science). An anti-histidine antibody (His Capture kit, GE Healthcare Life Science) was immobilized at approximate 14,500 RU onto the sensor chip CM-5 (GE Healthcare Life Science) using the Amine Coupling Kit (GE Healthcare Life Science) according to the protocol supplied by the manufacturer. Then, Histag H-PGDS was injected and captured on the chip at approximate 900 RU using PBS(-) as the running buffer. Running buffer was replaced with an assay buffer containing 20 mM HEPES (pH7.4), 150 mM NaCl, 2 mM $MgCl_2$, 2 mM GSH, 1% DMSO, and 0.005% Tween20. Test compounds were 2-fold serially diluted in the assay buffer and tested for binding to the captured Histag H-PGDS at a flow rate of 30 μl/min. The raw data (n=3) were processed by BIA evaluation Software (GE Healthcare Life Science). TFC-007, prepared according to JP2007-51121A, was purchased from HanChem Co., Ltd. (Daejeon, Korea) and used as a high-affinity control compound.

2.4 Additional purification and crystallization of human H-PGDS

Preparation of the human H-PGDS protein for crystallization was performed as reported.[24] Additional purification of the protein was performed as before to obtain high quality crystals, by chromatography on a SuperQ-5PW column (TOHSO). The eluted protein was concentrated to 5 mg/ml with an Amicon Ultra filter (Merck) equipped with YM-10 membrane. The sample thus obtained was washed with 20 mM Tris-HCl (pH 8.0) buffer.

Crystallization of the complex with F092 was performed by the counter diffusion method to avoid forming cluster crystals, using a Crystal Tube Kit (MB2004-CRT200, Confocal Science Inc., Tokyo, Japan).[25] An 8 μl aliquot of the protein solution, containing 2.5 mg/ml H-PGDS protein, 50 mM Tris-HCl (pH 8.5), 17.5% (w/v) PEG6000, 1 mM DTT, 1 mM GSH, 1 mM $MgCl_2$, and 1% dioxane was loaded into a glass capillary equipped with a 6 mm length gel-tube. The assembled capillary was placed into 1 ml of the reservoir solution, containing 50 mM Tris-HCl (pH 8.5), 35% (w/v) PEG6000, 2 mM DTT, 2 mM GSH, 2 mM $MgCl_2$, and 2% dioxane for several days. Single crystals of H-PGDS in complex with F092 were successfully obtained.

2.5 Data collection and structure determination

Diffraction data of the H-PGDS crystals in the complex with F092 were collected at 100 K on the i04 beam line at Diamond Light Source (Didcot, UK) using a camera system of

PILATUS6M. The crystals grown in the capillaries were extracted into the reservoir solution, soaked in a cryo-protectant solution containing 15% glycerol, and flash-cooled in a stream of nitrogen gas at 100 K prior to data collection. The diffraction images were integrated and scaled by iMOSFLM[26] and Aimless,[27] from the CCP4 suite.[28]

The complex structure was determined by the molecular replacement method with MOLREP[29] by using the native structure as the search model (PDB ID : 1IYH). The model re-building and the refinement of the structure were performed with Coot[30] and REFMAC5.[31] In this report, electron density peaks, with the threshold cutoff of 1.0σ and 3.0σ in the *2Fo-Fc* Fourier and the *Fo-Fc* omit-map, respectively, were picked up as candidates of water molecules. Then the candidates with appropriate hydrogen bond interactions with surrounding O and N atoms were selected and assigned as water molecules. Statistics of data collection and structure refinement are summarized in Table 2. The coordinates and structure factors have been deposited in the PDB, with the PDB ID: 5YWX.

2.7 QM calculations

The coordination sets of H-PGDS homodimers (residues 2-199 in chains A and B) deposited to the PDB as the F092 complex (5YWX) and the apo form (1IYH) were employed for the FMO calculations. Crystal water molecules within 4.5 Å from any receptor atoms were retained. N- and C-termini of the protein are in the form of $-NH_3^+$ and $-COO^-$, respectively.

Hydrogen atoms were added and concurrently optimized, using the Amber10: EHT force field implemented in MOE [*Molecular Operating Environment (MOE)*, 2016.08; Chemical Computing Group Inc., QC, Canada, 2016]. In the structure optimization process based on molecular mechanics, all heavy atoms were fixed at the X-ray structure coordinates. We then performed all FMO calculations[14, 21, 32] at the second-order Møller-Plesset perturbation theory (MP2) level with a 6-31G* basis set, using the ABINIT-MP program [*MIZUHO/BioStation Viewer*, version 3.0; Mizuho Information and Research Institute, Inc., Tokyo, Japan, 2013]. In our FMO calculations, each single amino acid unit containing side chain, Cα, and N-terminal side amide group, was assigned to a fragment. This fragmentation procedure is a default behavior of ABINIT-MP for accurate energy calculations. In addition, GSH, F092, and the Mg^{2+} ion were treated as single fragments. IFIE was used to reveal their energy contributions, and PIEDA[22, 23] was further used to analyze the each energy component of IFIE: electrostatic (ES), exchange-repulsion (EX), charge transfer with higher order mixed terms energies (CT+mix), and dispersion interaction (DI).

$$\Delta\tilde{E}_{IJ} = \Delta\tilde{E}_{IJ}^{\mathrm{ES}} + \Delta\tilde{E}_{IJ}^{\mathrm{EX}} + \Delta\tilde{E}_{IJ}^{\mathrm{CT+mix}} + \Delta\tilde{E}_{IJ}^{\mathrm{DI.}}. \qquad \textbf{Scheme 1}$$

In this equation, $\Delta\tilde{E}_{IJ}$ is the IFIE between *I*-th and *J*-th fragments and each item of addition is the energy component. Attractive and repulsive interactions are showed negative and positive

values for IFIE, respectively. Interactions of fragments in the chain A were used for the IFIE and PIEDA studies.

3 Results and Discussion

3.1 Design and synthesis of F092

Carron et al.[10] and Trujillo et al.[13] pointed out that the strong affinity for H-PGDS required the inhibitors to form a hydrogen bond with the conserved water molecule near Leu199. Thus, we aimed to design and synthesize a new compound that shares the typical substructures of H-PGDS inhibitors, a phenyl group and a heterocyclic group, and also interacts with the conserved water molecule. Referring to the substructures reported by Sanofi-Aventis, Astra-Zeneca, and Pfizer,[13] F092 was empirically designed to have an elongated backbone structure to fit the deep catalytic cavity (Fig. 1). We expected that the back bone structure of the pyrimidine next to the pyridine would be important for F092 to obtain strong interactions with the conserved water molecule by forming two hydrogen bondings between the O atom of the water and the two nitrogen atoms of the rings.

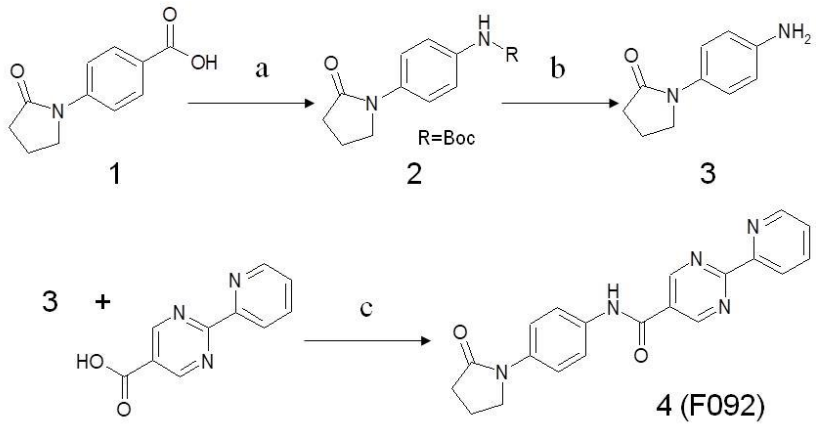

Fig. 1 Synthetic scheme of F092.
Reagents and conditions: (a) DPPA, Et_3N, *tert*-BuOH, toluene, 120 °C, 16.5 h; (b) HCl, 1,4-dioxane, rt, 3 h; (c) $T_3P^®$, Et_3N, CH_2Cl_2, rt, 1 h.

The synthesis scheme of F092 is shown in Fig. 1. The Curtius rearrangement of commercially available 4-(2-oxopyrrolidin-1-yl)benzoic acid (**1**), followed by HCl-mediated deprotection of the *N*-Boc, afforded 1-(4-aminophenyl)pyrrolidin-2-one (**3**). The aniline, **3,** was coupled with 2-(pyridin-2-yl)pyrimidine-5-carboxylic acid in the presence of propylphosphonic anhydride ($T_3P^®$) to produce F092 (**4**) in good yield.

As we expected, F092 had a high-affinity for human H-PGDS. The dissociation constant (K_D) of F092 from the purified human Histag H-PGDS determined by SPR was 0.14 nM $\pm$ 0.010 nM (Table 1). It was comparable to that of the known clinical candidate compound, TFC-007[1] (K_D = 0.37 $\pm$ 0.017 nM). We further confirmed that F092 strongly inhibited the enzyme activity of the purified H-PGDS (Aritake et al. unpublished results). Therefore, we studied the H-PGDS crystal structure in complex with F092 to analyze the interactions between ligand, protein, and water molecules.

Table 1 List of compounds discussed in this paper.

Compound	Structure	K_D (nM)*
TFC-007	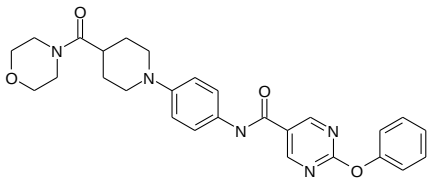	0.37 ± 0.017
F092	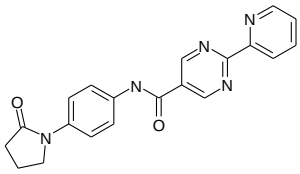	0.14 ± 0.010

*K_D values were determined from the results of triplicate SPR measurements.

3.2 Structure analysis of H-PGDS in complex with F092

The human H-PGDS crystals in complex with F092 diffracted to 1.74 Å (PDB ID: 5YWX, data statistics are shown in Table 2). F092 was located in the catalytic cavity and surrounded by Arg12, Arg14, and Thr159 in the inner cavity, Trp104 and GSH in the central cavity, and Trp39 and Ala105 in the peripheral region (Fig. 2). F092 interacted hydrophobically with Arg14 and Met99 in the inner cavity and Phe9 in the peripheral region. The pyrimidine ring of F092 formed typical π-π interactions with the indole side-chain of Trp104, because the pyrimidine ring was parallel to the indole ring (Fig. 2).

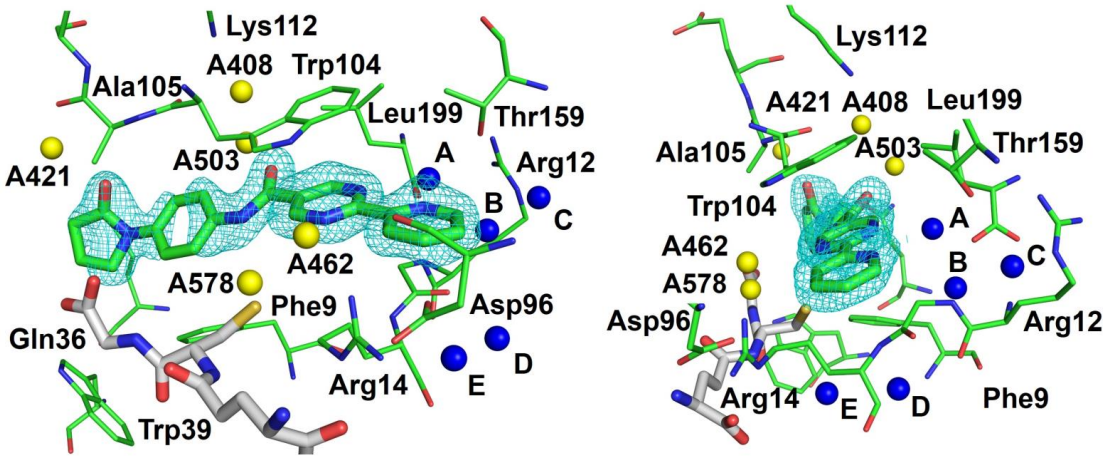

Fig. 2 Interactions between F092 and H-PGDS.
Views from two different directions are drawn schematically. Stick models show the refined model of F092 and GSH in the F092 complex (PDB ID: 5YWX, chain A). Blue meshes indicate the difference electron density of an *Fo-Fc* omit map of the bound F092 calculated at 3.0σ. Five blue spheres show the conserved water molecules ($Water_A$-$Water_E$) in the catalytic cavity. Their residue numbers shown in the PDB data (5YWX) are as follows: $Water_A$: HOHA442, $Water_B$: HOHA515, $Water_C$: HOHA464, $Water_D$: HOHA518, $Water_E$: HOHA482. Other five yellow spheres show the specific water molecules in the chain A of the F092 complex (HOHA408, HOHA421, HOHA462, HOHA503 and HOHA578).

Table 2. Data processing and refinement statistics.

	H-PGDS-F092 complex
Data collection	
Space Group	P1
Cell constants (Å)	*a*=47.0, *b*=48.2, *c*=91.0
	α=99.0, *β*=92.3, *γ*=90.0
No. of molecules in ASU	4
No. of crystals	1
Resolution Range (Å)	40.0- 1.74
No. of independent reflections	79,469
Completeness (%)	97.1 (95.6)
R_{merge} (I, %)	0.088 (0.523)
Average Mosaicity	0.42
I/σ(I) (%)	5.9 (1.9)
Refinement	
Non-hydrogen atoms	
Protein	6552

	Compound	108
	Solvent (H_2O)	583
Rwork value, Rfree value		0.203, 0.253
RMSD bond length (Å^2)		0.011
RMSD bond angles (^{o})		1.47
Mean B (protein) (Å^2)		
	Main Chain	22.1
	Side Chain	21.6
Mean B (solvent) (Å^2)		23.5
Mean B (compound) (Å^2)		22.4
Chiral center		0.081
Planar groups		0.008
VDW repulsions		0.246
PDB ID		5YWX

In the catalytic cavity of chain A of the F092 complex, total 10 water molecules were located within 6.0 Å from their interacting atoms of F092. Among them, five water molecules in the inner cavity were observed in all four chains contained in the crystal unit of the F092 complex. Thus, the five stable water molecules were named $Water_A$~$Water_E$. They are shown as blue spheres in Fig. 2. In addition to the stable water molecules, five specific water molecules, HOHA462, HOHA578, HOHA408, HOHA503, and HOHA421 were observed in the structure of chain A (shown as yellow spheres in Fig. 2). In the F092 complex structure, the averaged B-factor of the 5 stable water molecules ($Water_A$ ~ $Water_E$) was 9.0 Å^2. This value was much lower than that of the Cα atoms (20.7 Å^2) of the protein molecule. Contrary, the other water molecules observed in the central and peripheral regions (yellow spheres) had much higher

B-factors. Their averaged B-factor was 33.5 $Å^2$. This difference suggested that the five water molecules in the inner cavity of H-PGDS were fixed tightly to the protein surface.

Overlay of the crystal water molecules and interacting amino acids in the apo form (PDB ID: 1IYH) and the complex forms of H-PGDS (PDB IDs: 5YWX and 3KXO) are shown in Fig. 3. All chains of the reported apo form structure in common contained the five stable water molecules (shown as magenta spheres in Fig. 3). They were located at the same coordinates corresponding to the five stable water molecules ($Water_A$ ~ $Water_E$) in the F092 complex (shown as green spheres in Fig. 3). Thus, these water molecules ($Water_A$ ~ $Water_E$) are considerable as conserved water molecules. The conserved water molecules were also observed at the same positions in the crystals of the KXO complex[10] (shown as green spheres in Fig. 3). Fig. 3 also shows that $Water_A$ corresponds to "the primary water molecule near Leu199", and $Water_B$ corresponds to "the second water molecule" reported before.[10, 13]

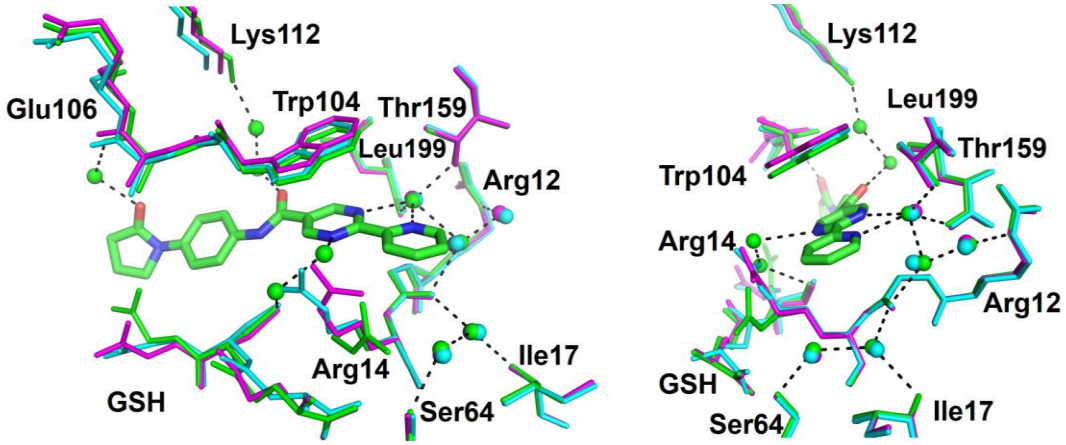

Fig. 3 Overlay of the crystal water molecules and interacting amino acids in the apo form and the complex forms of H-PGDS.
Views from two different directions are drawn schematically. Green sticks show the refined model of F092 surrounded by amino acid residues of the catalytic cavity. Lines and spheres colored with green, magenta and cyan show superposed structures of the F092 complex (5YWX, chain A), the apo form (1IYH, chain A) and the KXO complex (3KXO, chain A), respectively. Black dashed lines show hydrogen bonding interactions between these water molecules and the amino acid residues of the F092 complex.

F092 formed four hydrogen bonding networks containing $Water_A$-$Water_B$-$Water_C$, HOHA462-HOHA578, HOHA408-HOHA503, and HOHA421 (Figs. 2 and 3). In detail, $Water_A$ interacted with the carbonyl O atom of Leu199 and the Oγ atom of Thr159, and $Water_B$ formed a hydrogen bonding network with $Water_A$. $Water_C$ interacted with the Nε atom of Arg12. HOHA462 interacted with the Nη1 atom of Arg14, and HOHA578 interacted with the Sγ atom of the GSH molecule. HOHA408 interacted with Nζ atom of Lys 112, and HOHA503 interacted directly with the carbonyl O21 atom of F092. HOHA421 interacted with the carboxyl O atom of Ala105 and the carbonyl O27 atom of F092. $Water_A$ formed two hydrogen bonding interactions with the pyridine and pyrimidine N atoms of F092, at the distance of 2.88 Å and 2.92Å, respectively. The strong affinity of F092 for H-PGDS (Table 1) may be due to these direct hydrogen bonding interactions.

3.3 Analysis of interaction energies between F092, crystal waters and H-PGDS

3.3.1 Interactions between F092 and H-PGDS

The FMO calculations indicated that the lowest IFIE between F092 and H-PGDS fragments was observed with the attractive interaction between F092 and cofactor GSH (-53.03 kcal/mol). Since GSH consists of three amino acid units (Gly-Cys-Asp), it is plausible that the absolute value of the IFIE for F092 with GSH was larger than that with other fragments consisted of a single amino acid unit. In addition the sulfur atom of Cys of GSH formed a hydrogen bonding interaction with the ligand. The remarkably low IFIE indicated the key role of GSH in ligand-binding.

The IFIE values of the interactions between F092 and amino acid residues that located within 6.0 Å from the any atom of F092 are shown in Fig. 4. The IFIE values of interactions formed with Arg12, Gly13, Gln36, Asp96, Trp104, Lys112, Thr159, and Leu199 had large absolute values, as compared to those with the others. These interactions were important in F092 binding. Here we were aware that the IFIE value of the interaction between Leu199 and F092 was positive and especially high (10.09 kcal/mol). Thus, we wondered why F092 had a high affinity for H-PGDS, despite the strong repulsion of Leu199 calculated.

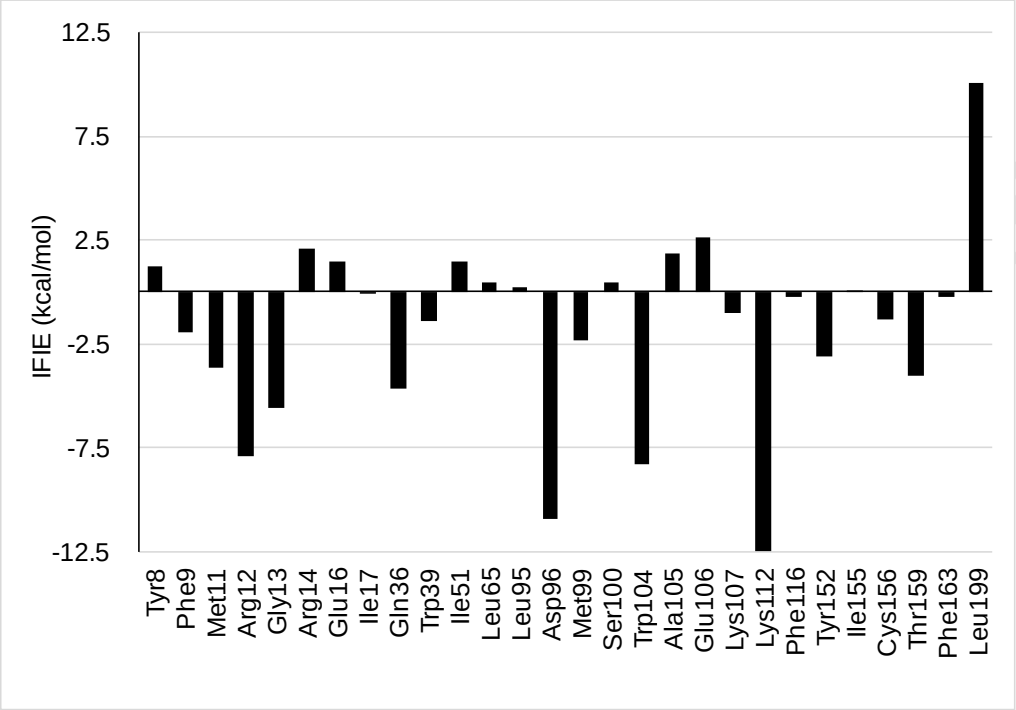

Fig. 4 IFIE values of the interactions between amino acid residues and ligands in the F092 complex.
The interactions between F092 and amino acid residues located within 6.0 Å from the any atom of the ligand were selected and their IFIE values were calculated.

To clarify which types of interactions were involved in the interactions, the PIEDA calculations were performed for the F092 complex. Figure 5 shows the distribution of the PIEDA of the interactions shown in Fig. 4. The ES values (shown in cyan bars) of the interactions of Asp96 and Lys112 with the ligand were both remarkable. The value of Asp96 was -9.73 kcal/mol, and that of Lys112 was -12.50 kcal/mol. Thus, interactions of these residues with F092 are dominated by the electrostatic binding. In contrast, highly repulsive ES values were observed with Arg14 (6.12 kcal/mol) and Leu199 (12.16 kcal/mol). These indicated that Arg14 and Leu199 are involved in electrostatically repulsive interactions for the ligand binding.

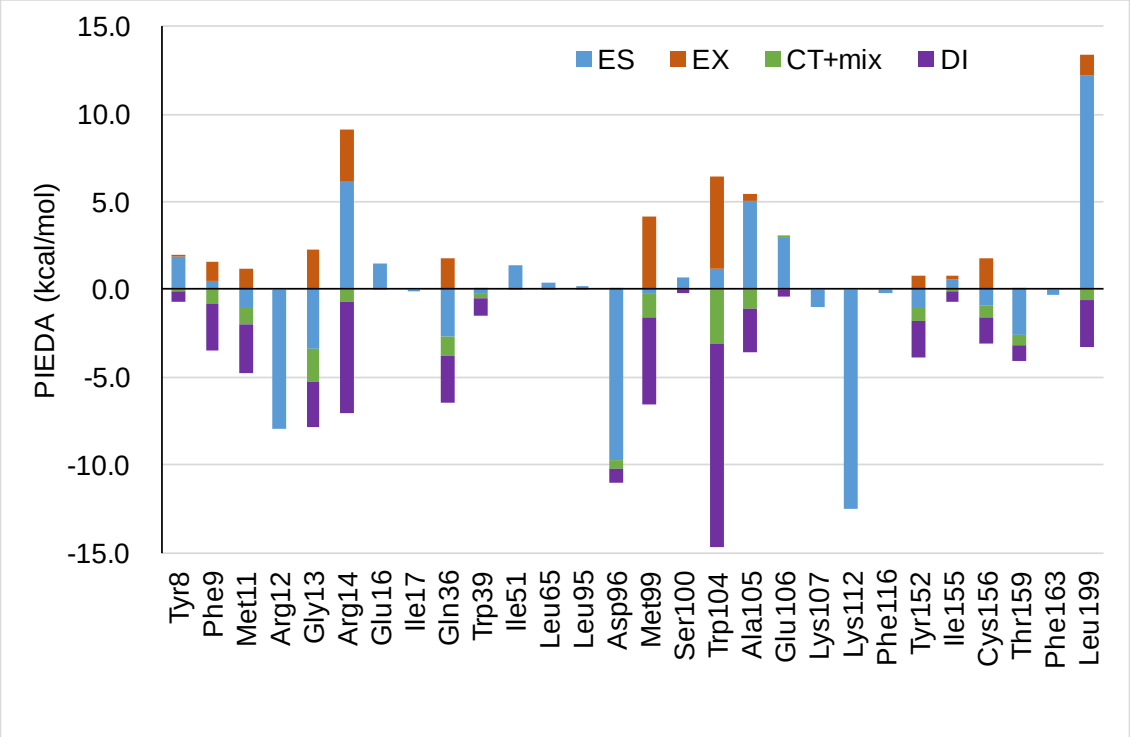

Fig. 5 Distribution of the PIEDA calculated with the F092 complex structure.
The interactions between amino acid residues and F092 shown in Fig. 4 were analyzed by the PIEDA method. The electrostatic interaction (ES), exchange-repulsion (EX), charge transfer with higher-order mixed terms energies (CT+mix), and dispersion interaction (DI) are represented by cyan, orange, green, and purple, respectively.

The interactions of F092 with Arg14, Met99, and Trp104 had large negative DI values (shown in purple bars), which meant that their dispersion interactions contributed to the F092 binding. These residues were hydrophobically interacted as described in Section 3.2. The PIEDA analysis quantitatively indicated the remarkable aromatic interactions that contributed to the ligand binding to H-PGDS. Summary of these interaction energy studies are represented in Fig. 6.

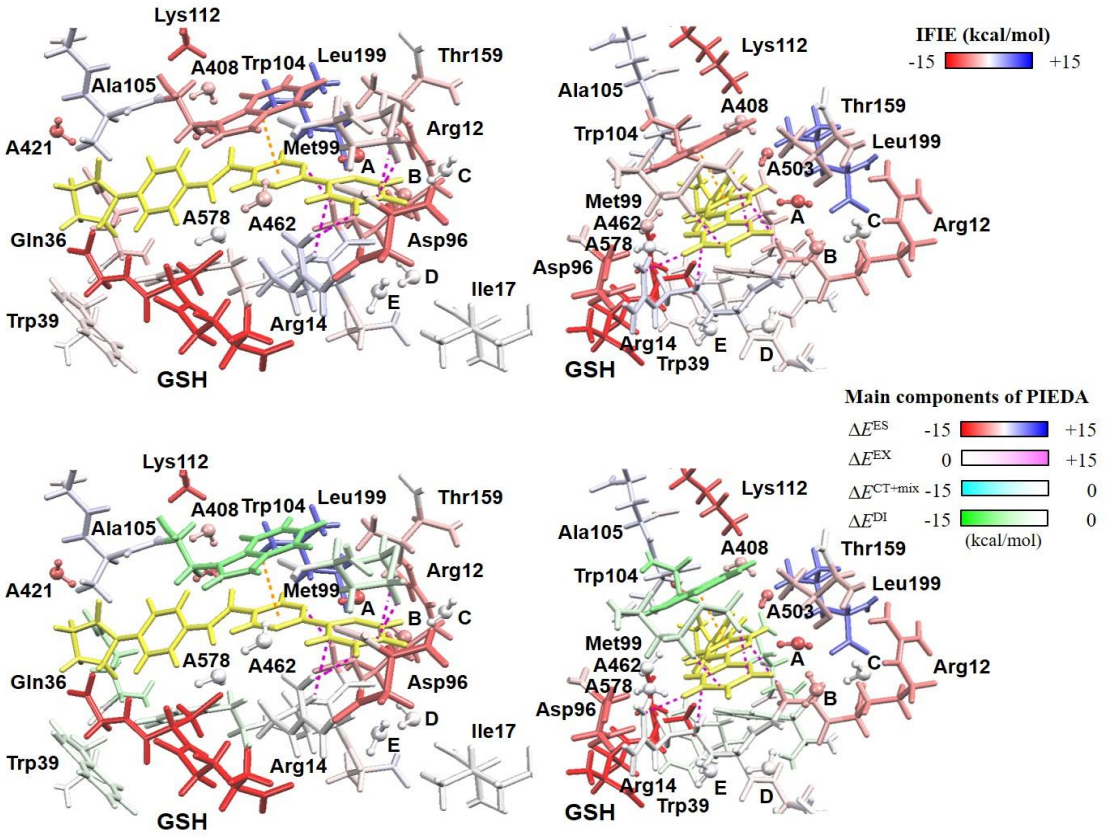

Fig. 6 Visualization of interaction energies of F092 with amino acid residues, water molecules, and GSH in the H-PGDS complex.
Figures in the top row show the summary of IFIE analysis for F092 fragment (shown in yellow). The fragments with attractive and repulsive interactions are represented by red and blue, respectively. Figures in the bottom row show the results of the PIEDA methods for F092 fragment (shown in yellow), the main components of the stabilizing interactions of fragments are represented by the following color scheme: ES, red and blue; EX, white and pink; CT+mix, light blue and white; DI, green and white. CH-p and p-p interactions are indicated by purple and orange dot lines, respectively, where they were analyzed using the CHPI program.[33]

3.3.2 Significant interactions between water molecules and H-PGDS

The IFIE values between each water molecule and all amino acid residues in the apo form (1IYH, chain A) and the F092 complex form (5YWX, chain A) were calculated by the FMO method. Amino acid residues significantly interacting with the each crystal water molecule are listed in Table 3. Significant interactions discussed in this paper were set to those with an

absolute IFIE values greater than or equal to 3.0 kcal/mol, which was an empirically threshold in FMO study reported before.[33] The lists of amino acids significantly interacting with the conserved water molecules were almost identical between the two coordinates except Arg14, whose side chain was rotated in the direction of $Water_A$ and $Water_E$ only in the F092 structure (Fig. 3).

Table 3. Significant interactions between the water molecules and amino acids in the catalytic cavities.

water	interacting amino acid*	
	1IYH	5YWX
$Water_A$	Leu199	Leu199, Thr159, Arg14
$Water_B$	Arg14, Arg12, Leu199	Arg14, Arg12
$Water_C$	Arg12, Cys156, Arg194	Arg12, Cys156, Arg194
$Water_D$	Arg14, Ile17, Ile18	Arg14, Ile17
$Water_E$	Ser64, Tyr152, Asp96	Ser64, Tyr152, Asp96, Arg14
HOHA408	−	Lys112, Ala105
HOHA421	−	Glu106, Lys107
HOHA462	−	Arg14, Trp104, Asp96
HOHA503	−	Lys112
HOHA578	−	Arg14

* Amino acids interacting to the water molecules with |IFIE| > 3 kcal/mol.

Among them, water-amino acid interaction pairs with the strongest energies were selected and listed with their IFIE values (Tables 4 and 5). In our fragmentation of FMO method, single amino acid fragment contains its side chain, Cα, and N-terminal side amide group, so that the FMO fragment unit is slightly different from the standard amino acid residue unit. The point should be noted when a carbonyl group of main chain closely related to the inter-fragment

interactions. For example, Arg14 fragment includes the carbonyl group of the peptide bond between Gly13 and Arg14, and Glu106 fragment includes that between Ala105 and Glu106. These strong interactions were almost indicated as hydrogen bindings in Fig. 3.

Table 4. IFIE values of the strongest water-amino acid interactions with each water molecule in the catalytic cavity of the apo form.

water-amino acid interaction*		IFIE (kcal/mol)
water	amino acid* (aa)	aa-water
$Water_A$	Leu199	-21.60
$Water_B$	Arg14	-8.70
$Water_C$	Arg12	-18.13
$Water_D$	Arg14	-8.27
$Water_E$	Ser64	-8.62

*Amino acid residue contributing to the strongest interaction with each water molecule.

Table 5. Related IFIE values of the strongest water-amino acid interactions with each water molecule in the catalytic cavity of the F092 complex form.

water-amino acid interaction		IFIE (kcal/mol)			
water	amino acid* (aa)	aa-water	water-F092	aa-F092	aa-water-F092**
$Water_A$	Leu199	-16.72	-11.54	10.09	-18.16
$Water_B$	Arg14	-9.68	-6.75	2.07	-14.35
$Water_C$	Arg12	-16.30	-0.09	-7.91	-24.29
$Water_D$	Arg14	-8.66	-0.65	2.07	-7.24
$Water_E$	Ser64	-8.06	0.76	0.30	-7.01
HOHA408	Lys112	-14.37	-4.67	-12.50	-31.54
HOHA421	Glu106	-11.15	-10.57	2.60	-19.13
HOHA462	Arg14	-12.00	-4.42	2.07	-14.35
HOHA503	Lys112	-4.94	-9.11	-12.50	-26.55
HOHA578	Arg14	-7.04	0.68	2.07	-4.29

* Amino acid residue contributing to the strongest interaction with each water molecule.

**The IFIE of aa-water-F092 shows summation of the IFIEs between aa-water, water-F092, and aa-F092.

The calculated IFIEs shown in the columns of "IFIE aa-water" confirmed that all of the conserved water molecules in both structures maintained their strong interactions with the surface amino acids of the H-PGDS catalytic cavity (< -8.06 kcal/mol), which was much lower than the reference threshold[33] of significant interactions. Especially, $Water_A$, and $Water_C$ showed remarkable stabilities.

Table 4 indicates that $Water_A$ is highly stable due to the strong interaction with Leu199 (-21.60 kcal/mol). The negative charge of carboxyl moiety of Leu199 at the C-terminus of H-PGDS might cause the strong interaction. And $Water_A$ is adjacent to the ligand binding site, thus it must be a key molecule to design high-affinity ligands. The calculated IFIE between Leu199 and $Water_A$ explained the results of Thorarensen's group,[13] which is "high affinity for H-PGDS would require ligands to form a hydrogen bond with $Water_A$ than to displace the water molecule".

As shown in the "IFIE aa-water" column of Table 5, specific five water molecules in the central and peripheral part of the catalytic cavity of the F092 complex also stably bound to the interacting amino acid residues (< -4.94 kcal/mol). FMO calculation indicated that HOHA408 and HOHA421 formed strong hydrogen bondings with Lys112 and Glu106 that existed in the peripheral solvent-exposed part of the C-terminal domain, and HOHA462 formed hydrogen bonding with Arg14 in the central cavity. The existence of the 5 additional stable water

molecules (yellow spheres in Fig. 2) in the central and peripheral part of the catalytic cavity and their formation of stable hydrogen bonding networks (section 3.3.3) explained our empirical results that compounds with an elongated backbone structure to fit from the deep inner cavity to the peripheral part of the cavity would have strong affinity to H-PGDS.

3.3.3 Hydrogen bonding networks of the water molecules in the F092 complex

The interaction energies between the 10 water molecules and F092 were calculated and shown in the "IFIE water-F092" column of Table 5. $Water_A$, $Water_B$, HOHA421 and HOHA503 had large attractive interactions with F092 (-11.54, -6.75, -10.57 and -9.11 kcal/mol, respectively). HOHA408 and HOHA462 also had significant interactions with F092. It indicated that these 6 crystal water molecules including ones locating in the central cavity and the peripheral part of the cavity, directly contributed to the stable ligand binding.

Addition to these direct interactions between water molecules and F092, interactions of hydrogen bonding networks including water molecules and F092 should be considered. The summation of IFIE values for the network interactions are indicated in the "IFIE aa-water-F092" column of Table 5, which are the sums of the three types of IFIE values, IFIEs between amino acid and water, water and F092, and amino acid and F092.

Table 5 indicates that Leu199 formed a strongly attractive interaction with $Water_A$ (-16.72 kcal/mol), and a strong repulsive interaction with F092 (10.09 kcal/mol) as pointed in the

section 3.3.1. But in the F092 complex, a hydrogen bonding network of Leu199-$Water_A$-F092 was formed, and its IFIE value ("IFIE aa-water-F092") was -18.16 kcal/mol. These data indicated that the stable $Water_A$ in H-PGDS formed a hydrogen bonding network and balanced the repulsive interaction between Leu199 and F092. This result reaffirmed that the stable water molecule, $Water_A$ is important for the robust ligand binding.

$Water_B$ also worked for constructing a stable hydrogen bonding network of Arg14-$Water_B$-F092 (-14.35 kcal/mol) in the F092 complex and overcoming the effects of repulsion between Arg14 and the ligand (2.07 kcal/mol). Despite $Water_C$ scarcely had an interaction with the ligand (-0.09 kcal/mol for F092), the Arg12-$Water_C$-F092 network was stable due to the two strongly attractive interactions between Arg12-$Water_C$ and Arg12-F092 (Table 5).

Specific five water molecules in the F092 complex also formed bridged hydrogen bonding networks with the interacting amino acid(s) and F092. IFIE values shown in the "aa-water-F092" column of Table 5 indicate that Lys112-HOHA408-F092, Lys112-HOHA503-F092, Glu106-HOHA421-F092, Arg14-HOHA462-F092, and Arg14-HOHA578-F092 networks largely contribute F092 binding (-31.54, -26.55, -19.13, -14.35, and -4.29 kcal/mol, respectively).

To clarify the complexity of HOHA462 and HOHA578 contribution to the F092 binding, we performed IFIE analyses and PIEDA calculations of their interactions (Table 6). HOHA462 interacted with Arg14 (-12.00 kcal/mol), HOHA578 (-7.09 kcal/mol), and F092 (-4.42 kcal/mol). HOHA578 interacted with GSH (-21.01 kcal/mol) and Arg14 (-7.04 kcal/mol). These interaction energies were more than twice the reference threshold of IFIE except that between HOHA578 and F092 (0.68 kcal/mol). From PIEDA analysis, the strong interaction among the water molecules, Arg14, and GSH were mainly contributed by ES components, indicating that they formed hydrogen bonding interactions. Consequently, in addition to the effect of the $Water_B$, the hydrogen bonding network of F092-GSH-HOHA578-HOHA462-Arg14 that functioned as one group having significant interaction energies also contributed to cancel out the repulsion force between Arg14 and F092.

Table 6. Interactions with HOHA462 and HOHA578 in the F092 complex.

water	interacting fragment	DIST* (Å)	IFIE (kcal/mol)	PIEDA (kcal/mol)			
				ES	EX	CT+mix	DI
HOHA462	Arg14	1.84	-12.00	-17.00	10.85	-3.19	-2.66
	HOHA578	2.10	-7.09	-7.45	2.90	-1.35	-1.19
	F092	2.12	-4.42	-3.78	4.02	-2.16	-2.51
HOHA578	HOHA462	2.10	-7.09	-7.45	2.90	-1.35	-1.19
	GSH	2.21	-21.01	-27.49	16.06	-5.56	-4.01
	Arg14	2.26	-7.04	-7.33	3.58	-1.48	-1.81
	F092	2.70	0.68	1.94	0.16	-0.65	-0.76

*"DIST" means minimum distance (Å) between the two fragments. Hydrogen atoms were included in the distance calculation.

These analyses highlighted the importance of the hydrogen bonding networks including HOHA462 and HOHA578. To confirm the calculation there may be two types of researches. One is point mutation study with Arg14 to disrupt forming the hydrogen bondings. But the point mutation might cause a change in the overall structure of H-PGDS.[25] Thus energy study should be performed carefully after crystallization and determination of the structures of the mutant protein.

Another is ligand based study determining the binding affinity of the series of inhibitors as reported before by Trujillo et al..[13] Some substituents of F092 that displace HOHA462 or HOHA578 would rather decrease its binding affinity for H-PGDS. For example, a nitrile group attached at the C3 position of the pyridine, which would displace the water molecule HOHA462, is a promising substituent. Since HOHA578 is accessible with both substituents at the C3 position on pyridine and the C4 position on the pyrimidine ring, cyclic structures that form the linkage between the pyridine and pyrimidine ring with appropriate functionalities potentially displace both HOHA462 and HOHA578. We would like to synthesize these compounds, study their affinities for H-PGDS, and analyze their complex structures to answer this question in the future.

4 Conclusions

FMO studies of the interactions in a high-affinity inhibitor complex of human H-PGDS indicated that 6 water molecules locating from the deep inner cavity to the peripheral part of the cavity directly and significantly contributed to the ligand binding. Hydrogen bonding networks with the adjacent crystal waters eliminated the repulsive interactions between the surface amino acids and the ligand. This paper explained that compounds with an elongated backbone structure to fit from the deep inner cavity to the peripheral part of the cavity would have strong affinity to H-PGDS.

Acknowledgements

This work was supported in part by a grant from the Adaptable and Seamless Technology Transfer Program through Target-driven R&D, from the Japan Science and Technology Agency, to Y. U. and A. T. We sincerely thank to Dr. T. Fukami (RIKEN) for fruitful discussions.

Declarations of interest: none

References

1. Nabe T, Kuriyama Y, Mizutani N, Shibayama S, Hiromoto A, Fujii M, Tanaka K, Kohno S. Inhibition of hematopoietic prostaglandin D synthase improves allergic nasal blockage in guinea pigs. *Prostaglandins Other Lipid Mediat.* 2011; 95: 27-34.

2. Kajiwara D, Aoyagi H, Shigeno K, Togawa M, Tanaka K, Inagaki N, Miyoshi K. Role of hematopoietic prostaglandin D synthase in biphasic nasal obstruction in guinea pig model of experimental allergic rhinitis. *Eur. J. Pharmacol.* 2011; 667: 389-395.

3. Urade Y, Hayaishi O. Prostaglandin D2 and sleep/wake regulation. *Sleep Med Rev.* 2011; 15: 411-418.

4. Kaushik MK, Aritake K, Kamauchi S, Hayaishi O, Huang ZL, Lazarus M, Urade Y. Prostaglandin D(2) is crucial for seizure suppression and postictal sleep. *Exp. Neurol.* 2014; 253: 82-90.

5. Mohri I, Aritake K, Taniguchi H, Sato Y, Kamauchi S, Nagata N, Maruyama T, Taniike M, Urade Y. Inhibition of prostaglandin D synthase suppresses muscular necrosis. *Am. J. Pathol.* 2009; 174: 1735-1744.

6. Inoue T, Irikura D, Okazaki N, Kinugasa S, Matsumura H, Uodome N, Yamamoto M, Kumasaka T, Miyano M, Kai Y, Urade Y. Mechanism of metal activation of human hematopoietic prostaglandin D synthase. *Nat. Struct. Biol.* 2003; 10: 291-296.

7. Kanaoka Y, Ago H, Inagaki E, Nanayama T, Miyano M, Kikuno R, Fujii Y, Eguchi N, Toh H, Urade Y, Hayaishi O. Cloning and crystal structure of hematopoietic prostaglandin D synthase. *Cell.* 1997; 90: 1085-1095.

8. Hohwy M, Spadola L, Lundquist B, Hawtin P, Dahmen J, Groth-Clausen I, Nilsson E, Persdotter S, von Wachenfeldt K, Folmer RH, Edman K. Novel prostaglandin D synthase inhibitors generated by fragment-based drug design. *J. Med. Chem.* 2008; 51: 2178-2186.

9. Inoue T, Okano Y, Kado Y, Aritake K, Irikura D, Uodome N, Okazaki N, Kinugasa S, Shishitani H, Matsumura H, Kai Y, Urade Y. First determination of the inhibitor complex structure of human hematopoietic prostaglandin D synthase. *J Biochem.* 2004; 135: 279-283.

10. Carron CP, Trujillo JI, Olson KL, Huang W, Hamper BC, Dice T, Neal BE, Pelc MJ, Day JE, Rohrer DC, Kiefer JR, Moon JB, Schweitzer BA, Blake TD, Turner SR, Woerndle R, Case BL, Bono CP, Dilworth VM, Funckes-Shippy CL, Hood BL, Jerome GM, Kornmeier CM, Radabaugh MR, Williams ML, Davies MS, Wegner CD, Welsch DJ, Abraham WM, Warren CJ, Dowty ME, Hua F, Zutshi A, Yang JZ, Thorarensen A. Discovery of an Oral Potent Selective Inhibitor of Hematopoietic Prostaglandin D Synthase (HPGDS). *Acs Medicinal Chemistry Letters.* 2010; 1: 59-63.

11. Aritake K, Kado Y, Inoue T, Miyano M, Urade Y. Structural and functional characterization of HQL-79, an orally selective inhibitor of human hematopoietic prostaglandin D synthase. *J. Biol. Chem.* 2006; 281: 15277-15286.

12. Edfeldt F, Evenas J, Lepisto M, Ward A, Petersen J, Wissler L, Rohman M, Sivars U, Svensson K, Perry M, Feierberg I, Zhou XH, Hansson T, Narjes F. Identification of indole inhibitors of human hematopoietic prostaglandin D2 synthase (hH-PGDS). *Bioorg. Med. Chem. Lett.* 2015; 25: 2496-2500.

13. Trujillo JI, Kiefer JR, Huang W, Day JE, Moon J, Jerome GM, Bono CP, Kornmeier CM, Williams ML, Kuhn C, Rennie GR, Wynn TA, Carron CP, Thorarensen A. Investigation of

the binding pocket of human hematopoietic prostaglandin (PG) D2 synthase (hH-PGDS): a tale of two waters. *Bioorg. Med. Chem. Lett.* 2012; 22: 3795-3799.

14. Fedorov DG, Kitaura K, The Fragment Molecular Orbital Method: Practical Application to Large Molecular System, CRC Press, Boca Raton, FL, 2009.

15. Yoshida T, Fujita T, Chuman H. Novel Quantitative Structure-Activity Studies of HIV-1 Protease Inhibitors of the Cyclic Urea Type Using Descriptors Derived from Molecular Dynamics and Molecular Orbital Calculations. *Current Computer-Aided Drug Design.* 2009; 5: 38-55.

16. Yoshida T, Yamagishi K, Chuman H. QSAR study of cyclic urea type HIV-1PR inhibitors using ab initio MO calculation of their complex structures with HIV-1PR. *Qsar & Combinatorial Science.* 2008; 27: 694-703.

17. Hitaoka S, Harada M, Yoshida T, Chuman H. Correlation analyses on binding affinity of sialic acid analogues with influenza virus neuraminidase-1 using ab initio MO calculations on their complex structures. *J Chem Inf Model.* 2010; 50: 1796-1805.

18. Hitaoka S, Matoba H, Harada M, Yoshida T, Tsuji D, Hirokawa T, Itoh K, Chuman H. Correlation analyses on binding affinity of sialic acid analogues and anti-influenza drugs with human neuraminidase using ab initio MO calculations on their complex structures--LERE-QSAR analysis (IV). *J Chem Inf Model.* 2011; 51: 2706-2716.

19. Watanabe C, Fukuzawa K, Okiyama Y, Tsukamoto T, Kato A, Tanaka S, Mochizuki Y, Nakano T. Three- and four-body corrected fragment molecular orbital calculations with a novel subdividing fragmentation method applicable to structure-based drug design. *J. Mol. Graph. Model.* 2013; 41: 31-42.

20. Nakanishi I, Fedorov DG, Kitaura K. Molecular recognition mechanism of FK506 binding protein: an all-electron fragment molecular orbital study. *Proteins.* 2007; 68: 145-158.

21. Tanaka S, Mochizuki Y, Komeiji Y, Okiyama Y, Fukuzawa K. Electron-correlated fragment-molecular-orbital calculations for biomolecular and nano systems. *Physical Chemistry Chemical Physics.* 2014; 16: 10310-10344.

22. Tsukamoto T, Kato K, Kato A, Nakano T, Mochizuki Y, Fukuzawa K. Implementation of Pair Interaction Energy Decomposition Analysis and Its Applications to Protein-Ligand Systems. *J. Comput. Chem. Jpn. .* 2015; 14: 1-9.

23. Fedorov DG, Kitaura K. Pair interaction energy decomposition analysis. *Journal of Computational Chemistry.* 2007; 28: 222-237.

24. Takahashi S, Tsurumura T, Aritake K, Furubayashi N, Sato M, Yamanaka M, Hirota E, Sano S, Kobayashi T, Tanaka T, Inaka K, Tanaka H, Urade Y. High-quality crystals of human haematopoietic prostaglandin D synthase with novel inhibitors. *Acta Crystallogr*

Sect F Struct Biol Cryst Commun. 2010; 66: 846-850.

25. Pinzar E, Miyano M, Kanaoka Y, Urade Y, Hayaishi O. Structural basis of hematopoietic prostaglandin D synthase activity elucidated by site-directed mutagenesis. *J. Biol. Chem.* 2000; 275: 31239-31244.

26. Battye TG, Kontogiannis L, Johnson O, Powell HR, Leslie AG. iMOSFLM: a new graphical interface for diffraction-image processing with MOSFLM. *Acta Crystallogr D Biol Crystallogr.* 2011; 67: 271-281.

27. Evans PR, Murshudov GN. How good are my data and what is the resolution? *Acta Crystallogr D Biol Crystallogr.* 2013; 69: 1204-1214.

28. Winn MD, Ballard CC, Cowtan KD, Dodson EJ, Emsley P, Evans PR, Keegan RM, Krissinel EB, Leslie AG, McCoy A, McNicholas SJ, Murshudov GN, Pannu NS, Potterton EA, Powell HR, Read RJ, Vagin A, Wilson KS. Overview of the CCP4 suite and current developments. *Acta Crystallogr D Biol Crystallogr.* 2011; 67: 235-242.

29. Vagin A, Teplyakov A. MOLREP: an automated program for molecular replacement. *Journal of Applied Crystallography.* 1997; 30: 1022-1025.

30. Emsley P, Lohkamp B, Scott WG, Cowtan K. Features and development of Coot. *Acta Crystallogr D Biol Crystallogr.* 2010; 66: 486-501.

31. Murshudov GN, Skubak P, Lebedev AA, Pannu NS, Steiner RA, Nicholls RA, Winn MD, Long F, Vagin AA. REFMAC5 for the refinement of macromolecular crystal structures. *Acta Crystallogr D Biol Crystallogr.* 2011; 67: 355-367.

32. Kitaura K, Ikeo E, Asada T, Nakano T, Uebayasi M. Fragment molecular orbital method: an approximate computational method for large molecules. *Chemical Physics Letters.* 1999; 313: 701-706.

33. Heifetz A, Chudyk EI, Gleave L, Aldeghi M, Cherezov V, Fedorov DG, Biggin PC, Bodkin MJ. The Fragment Molecular Orbital Method Reveals New Insight into the Chemical Nature of GPCR-Ligand Interactions. *Journal of chemical information and modeling.* 2016; 56: 159-172.

34. Umezawa Y, Nishio M. CH/pi interactions as demonstrated in the crystal structure of guanine-nucleotide binding proteins, Src homology-2 domains and human growth hormone in complex with their specific ligands. *Bioorg. Med. Chem.* 1998; 6: 493-504.

Figure Legends

Fig.1 Synthetic scheme of F092.

Reagents and conditions: (a) DPPA, Et_3N, *tert*-BuOH, toluene, 120 ºC, 16.5 h; (b) HCl, 1,4-dioxane, rt, 3 h; (c) $T_3P^{®}$, Et_3N, CH_2Cl_2, rt, 1 h.

Fig. 2 Interactions between F092 and H-PGDS.

Views from two different directions are drawn schematically. Stick models show the refined model of F092 and GSH in the F092 complex (PDB ID: 5YWX, chain A). Blue meshes indicate the difference electron density of an *Fo-Fc* omit map of the bound F092 calculated at 3.0σ. Five blue spheres show the conserved water molecules ($Water_A$-$Water_E$) in the catalytic cavity. Their residue numbers shown in the PDB data (5YWX) are as follows: $Water_A$: HOHA442, $Water_B$: HOHA515, $Water_C$: HOHA464, $Water_D$: HOHA518, $Water_E$: HOHA482. Other five yellow spheres show the specific water molecules in the chain A of the F092 complex (HOHA408, HOHA421, HOHA462, HOHA503 and HOHA578).

Fig. 3 Overlay of the crystal water molecules and interacting amino acids in the apo form and the complex forms of H-PGDS.

Views from two different directions are drawn schematically. Green sticks show the refined model of F092 surrounded by amino acid residues of the catalytic cavity. Lines and spheres colored with green, magenta and cyan show superposed structures of the F092 complex (5YWX, chain A), the apo form (1IYH, chain A) and the KXO complex (3KXO, chain A), respectively.

Black dashed lines show hydrogen bonding interactions between these water molecules and the amino acid residues of the F092 complex.

Fig. 4 IFIE values of the interactions between amino acid residues and ligands in the F092 complex.

The interactions between F092 and amino acid residues located within 6.0 Å from the any atom of the ligand were selected and their IFIE values were calculated.

Fig. 5 Distribution of the PIEDA calculated with the F092 complex structure.

The interactions between amino acid residues and F092 shown in Fig. 4 were analyzed by the PIEDA method. The electrostatic interaction (ES), exchange-repulsion (EX), charge transfer with higher-order mixed terms energies (CT+mix), and dispersion interaction (DI) are represented by cyan, orange, green, and purple, respectively.

Fig. 6 Visualization of interaction energies of F092 with amino acid residues, water molecules, and GSH in the H-PGDS complex.

Figures in the top row show the summary of IFIE analysis for F092 fragment (shown in yellow). The fragments with attractive and repulsive interactions are represented by red and blue, respectively. Figures in the bottom row show the results of the PIEDA methods for F092 fragment (shown in yellow), the main components of the stabilizing interactions of fragments are represented by the following color scheme: ES, red and blue; EX, white and pink; CT+mix,

light blue and white; DI, green and white. CH-π and π-π interactions are indicated by purple and orange dot lines, respectively, where they were analyzed using the CHPI program.[34]

Table 1 List of compounds discussed in this paper.

Compound	Structure	K_D (nM)*
TFC-007	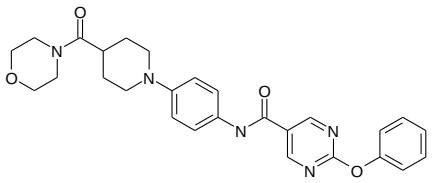	0.37 ± 0.017
F092	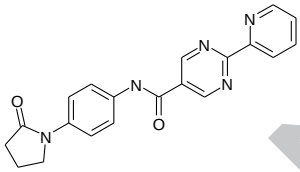	0.14 ± 0.010

*K_D values were determined from the results of triplicate SPR measurements.

Table 2. Data processing and refinement statistics.

H-PGDS-F092 complex		
Data collection		
Space Group		P1
Cell constants (Å)		*a*=47.0, *b*=48.2, *c*=91.0
		α=99.0, β=92.3, γ=90.0
No. of molecules in ASU		4
No. of crystals		1
Resolution Range (Å)		40.0- 1.74
No. of independent reflections		79,469
Completeness (%)		97.1 (95.6)
R_{merge} (I, %)		0.088 (0.523)
Average Mosaicity		0.42
I/σ(I) (%)		5.9 (1.9)
Refinement		
Non-hydrogen atoms		
	Protein	6552
	Compound	108
	Solvent (H_2O)	583
Rwork value, Rfree value		0.203, 0.253
RMSD bond length ($Å^2$)		0.011
RMSD bond angles (^{o})		1.47
Mean B (protein) ($Å^2$)		
	Main Chain	22.1
	Side Chain	21.6
Mean B (solvent) ($Å^2$)		23.5
Mean B (compound) ($Å^2$)		22.4
Chiral center		0.081
Planar groups		0.008
VDW repulsions		0.246
PDB ID		5YWX

Table 3. Significant interactions between the water molecules and amino acids in the catalytic cavities.

water	interacting amino acid*	
	1IYH	5YWX
$Water_A$	Leu199	Leu199, Thr159, Arg14
$Water_B$	Arg14, Arg12, Leu199	Arg14, Arg12
$Water_C$	Arg12, Cys156, Arg194	Arg12, Cys156, Arg194
$Water_D$	Arg14, Ile17, Ile18	Arg14, Ile17
$Water_E$	Ser64, Tyr152, Asp96	Ser64, Tyr152, Asp96, Arg14
HOHA408	−	Lys112, Ala105
HOHA421	−	Glu106, Lys107
HOHA462	−	Arg14, Trp104, Asp96
HOHA503	−	Lys112
HOHA578	−	Arg14

* Amino acids interacting to the water molecules with |IFIE| > 3 kcal/mol.

Table 4. IFIE values of the strongest water-amino acid interactions with each water molecule in the catalytic cavity of the apo form.

water-amino acid interaction*		IFIE (kcal/mol)
water	amino acid* (aa)	aa-water
$Water_A$	Leu199	-21.60
$Water_B$	Arg14	-8.70
$Water_C$	Arg12	-18.13
$Water_D$	Arg14	-8.27
$Water_E$	Ser64	-8.62

*Amino acid residue contributing to the strongest interaction with each water molecule.

Table 5. Related IFIE values of the strongest water-amino acid interactions with each water molecule in the catalytic cavity of the F092 complex form.

water-amino acid interaction		IFIE (kcal/mol)			
water	amino acid* (aa)	aa-water	water-F092	aa-F092	aa-water-F092**
$Water_A$	Leu199	-16.72	-11.54	10.09	-18.16
$Water_B$	Arg14	-9.68	-6.75	2.07	-14.35
$Water_C$	Arg12	-16.30	-0.09	-7.91	-24.29
$Water_D$	Arg14	-8.66	-0.65	2.07	-7.24
$Water_E$	Ser64	-8.06	0.76	0.30	-7.01
HOHA408	Lys112	-14.37	-4.67	-12.50	-31.54
HOHA421	Glu106	-11.15	-10.57	2.60	-19.13
HOHA462	Arg14	-12.00	-4.42	2.07	-14.35
HOHA503	Lys112	-4.94	-9.11	-12.50	-26.55
HOHA578	Arg14	-7.04	0.68	2.07	-4.29

* Amino acid residue contributing to the strongest interaction with each water molecule.

**The IFIE of aa-water-F092 shows summation of the IFIEs between aa-water, water-F092, and aa-F092.

Table 6. Interactions with HOHA462 and HOHA578 in the F092 complex.

water	interacting fragment	DIST* (Å)	IFIE (kcal/mol)	PIEDA (kcal/mol)			
				ES	EX	CT+mix	DI
HOHA462	Arg14	1.84	-12.00	-17.00	10.85	-3.19	-2.66
	HOHA578	2.10	-7.09	-7.45	2.90	-1.35	-1.19
	F092	2.12	-4.42	-3.78	4.02	-2.16	-2.51
HOHA578	HOHA462	2.10	-7.09	-7.45	2.90	-1.35	-1.19
	GSH	2.21	-21.01	-27.49	16.06	-5.56	-4.01
	Arg14	2.26	-7.04	-7.33	3.58	-1.48	-1.81
	F092	2.70	0.68	1.94	0.16	-0.65	-0.76

*"DIST" means minimum distance (Å) between the two fragments. Hydrogen atoms were included in the distance calculation.

Graphical abstract

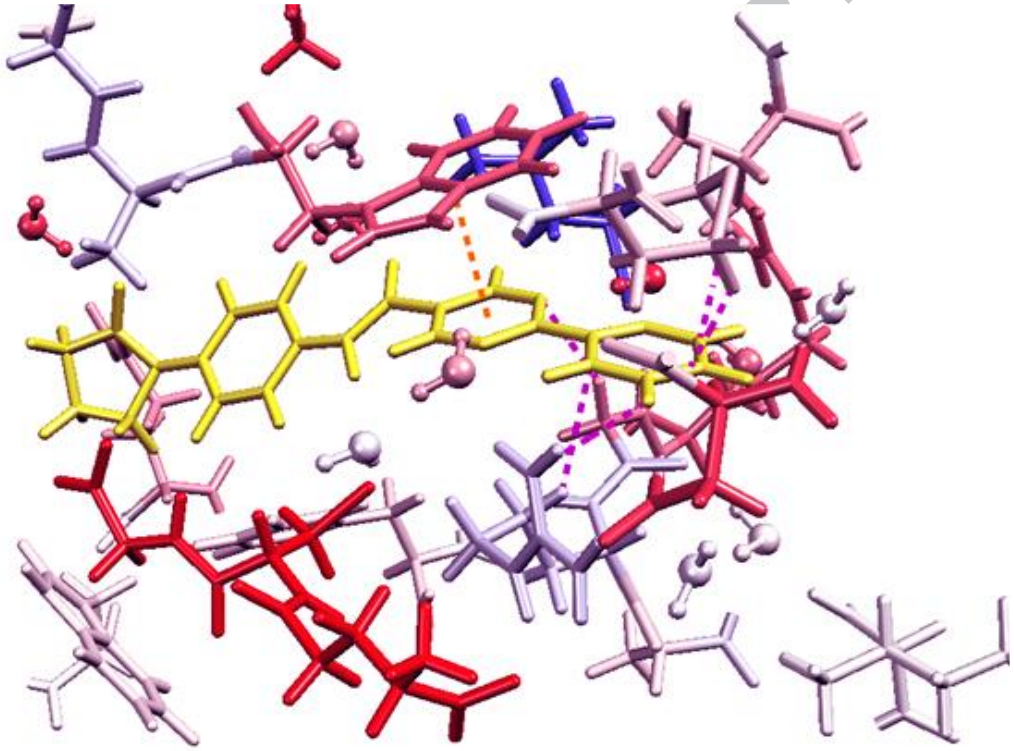

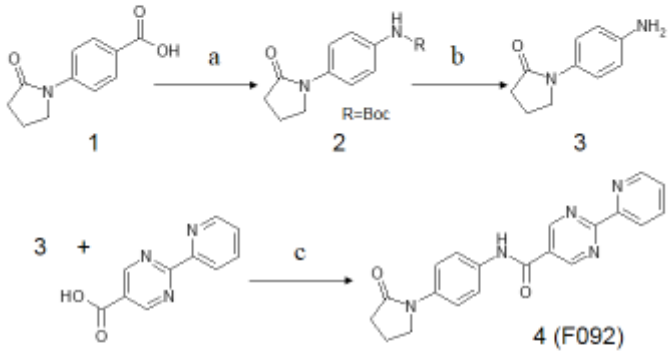

Fig.1 Synthetic scheme of F092.

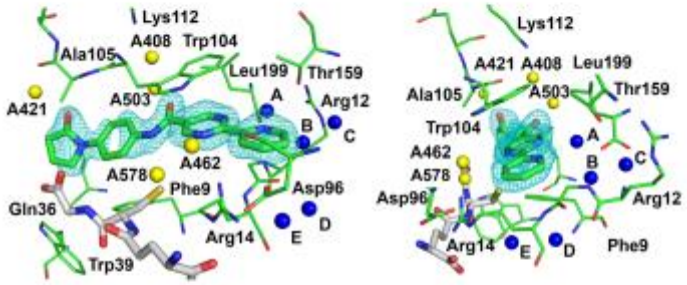

Fig. 2 Interactions between F092 and H-PGDS.

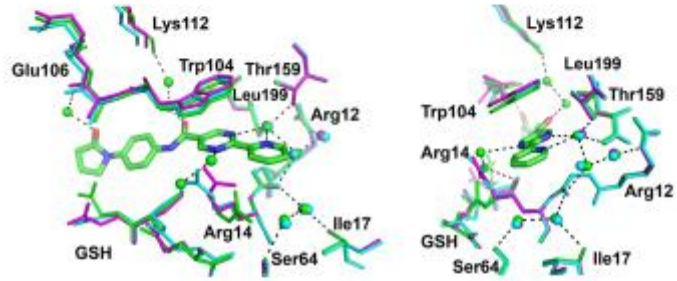

Fig. 3 Overlay of the crystal water molecules and interacting amino acids in the apo form and the complex forms of H-PGDS.

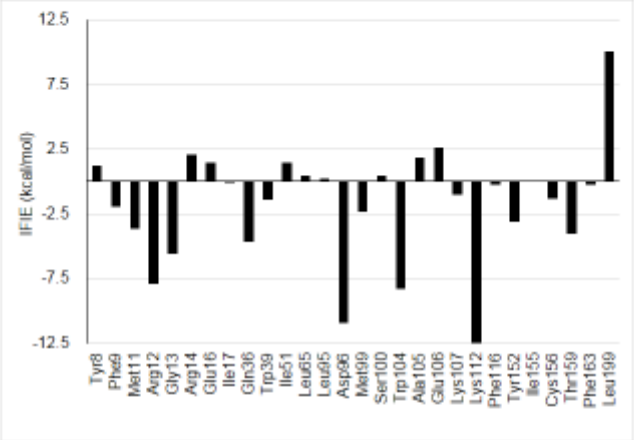

Fig. 4 IFIE values of the interactions between amino acid residues and ligands in the F092 complex.

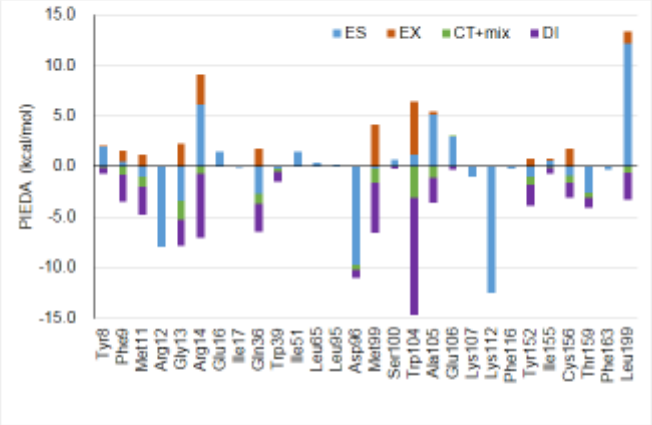

Fig. 5 Distribution of the PIEDA calculated with the F092 complex structure.

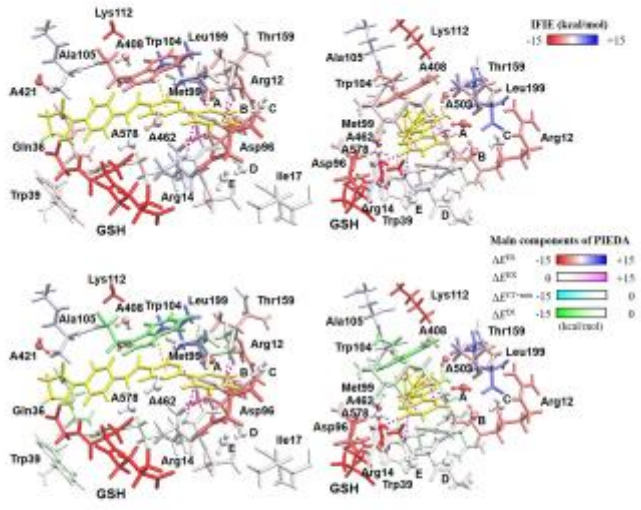

Fig. 6 Summary of interactions of fragments in the F092 complex.